

# Coupled-channel treatment of ${}^7\text{Li}(n, \gamma){}^8\text{Li}$ in effective field theory

Renato Higa,<sup>1,\*</sup> Pradeepa Premarathna,<sup>2,†</sup> and Gautam Rupak<sup>2,‡</sup>

<sup>1</sup>*Instituto de Física, Universidade de São Paulo,  
R. do Matão Nr.1371, 05508-090, São Paulo, SP, Brazil*

<sup>2</sup>*Department of Physics & Astronomy and HPC<sup>2</sup> Center for Computational Sciences,  
Mississippi State University, Mississippi State, MS 39762, USA*

## Abstract

The E1 contribution to the capture reaction  ${}^7\text{Li}(n, \gamma){}^8\text{Li}$  is calculated at low energies. We employ a coupled-channel formalism to account for the  ${}^7\text{Li}^*$  excited core contribution. The halo effective field theory calculations show that the contribution of the  ${}^7\text{Li}^*$  degree of freedom is negligible at momenta below 1 MeV and significant only beyond the  $3^+$  resonance energy, though still compatible with a next-to-next-to-leading order correction. A power counting that accounts for the size of this correction is proposed. We compare our formalism with a previous halo effective field theory [Zhang, Nollett, and Phillips, Phys. Rev. C **89**, 024613 (2014)] that also treated the  ${}^7\text{Li}^*$  core as an explicit degree of freedom. Our formal expressions and analysis disagree with this earlier work in several aspects.

Keywords: Coupled-channel, excited core, radiative capture, halo effective field theory

---

\* higa@if.usp.br

† psp63@msstate.edu

‡ grupak@ccs.msstate.edu

## I. INTRODUCTION

Radiative capture reactions with light nuclei sharpen our knowledge about the primordial evolution of our universe, the fuel in the interior of stars, and explosive phenomena of astrophysical objects [1–3]. Among them features the long-studied  ${}^7\text{Be}(p, \gamma){}^8\text{B}$  reaction, crucial in determining the flux of solar neutrinos that oscillate into different lepton flavors on their way to detection in Earth. The impact to neutrino oscillations and to the standard solar model of this reaction depends on the information of the respective cross section around the Gamow energy  $\sim 20$  keV. The Coulomb repulsion at such low energies makes it extremely difficult, if not impossible, for direct measurements in laboratory, which are presently limited to as low as  $\sim 100$  keV. Therefore, theoretical guidance for reliable extrapolations of experimental data down to energies of astrophysical interest is an unavoidable necessity. The mirror-symmetry, backed by the accidental isospin symmetry of quantum chromodynamics (QCD) at low energies, is often invoked to constrain the strong nuclear part of the reaction. Besides the mirror connection, the  ${}^7\text{Li}(n, \gamma){}^8\text{Li}$  reaction may reveal its importance in some astrophysical scenarios, such as inhomogeneous Big-Bang nucleosynthesis or neutron-rich explosive environments [1, 4].

Experimental studies on the  ${}^7\text{Li}(n, \gamma){}^8\text{Li}$  reaction date back to the 40’s [5] followed by a handful others between the 90’s and 2010’s [6–10]. Due to the absence of the Coulomb repulsion, many measurements were done in the sub-keV region with good precision, thus serving as testbed for theoretical low-energy extrapolations. Theoretical descriptions of this reaction vary in degree of sophistication and accuracy — *ab initio*/microscopic models [11–14] are tied to the choice of two- and three-nucleon interactions and numerical precision of the method whereas two-body [15–22] and three-body [23, 24] cluster configuration with phenomenological potentials are much simpler and more flexible with adjustable parameters to data. Halo/cluster effective field theory (halo EFT) relies on the same cluster approach, but uses quantum field theory techniques and a small momentum ratio to provide a model-independent, systematic and improvable expansion with controlled theoretical uncertainties. Halo EFT ideas emerge from Refs. [25, 26] and were extended to several loosely-bound nuclear systems (see Refs. [27–29] and references therein).

Halo EFT was first applied to  ${}^7\text{Li}(n, \gamma){}^8\text{Li}$  reaction in [30], which pointed out inconsistencies of potential-model extrapolations of fitted high-energy data to low energies, its origin, and ways to overcome it. The follow-up work [31] included E1 capture to the  $1^+$  state of  ${}^8\text{Li}$  and M1 capture from the initial  $3^+$  resonant state, while the effects of the  $\frac{1}{2}^-$   ${}^7\text{Li}$  excited-core state was argued to be of higher-order. A subsequent work by Zhang, Nollett, and Phillips [32] combined halo EFT formalism with asymptotic normalization coefficients (ANCs) obtained from *ab initio* variational Monte Carlo (VMC) method. Zhang *et al.* considered only E1 transitions, but included the  $\frac{1}{2}^-$  excited state of  ${}^7\text{Li}$  as an explicit degree of freedom. Their overall results are qualitatively similar to ours within the leading-order (LO) theoretical uncertainties. They also find the contribution of the excited core of  ${}^7\text{Li}$  compatible with a next-to-leading order (NLO) correction, meeting the expectations of our initial assumptions [31].

Nevertheless, Zhang *et al.* raised critical comments to our work, namely, (a) that the excited state of  ${}^7\text{Li}$  must be formally included in a LO calculation given its excitation energy of  $\sim 0.5$  MeV, smaller than the  $\sim 2$  MeV neutron separation energy of  ${}^8\text{Li}$ , (b) that the couplings of the different final state spin channels were made equal, which influences the rate of total initial spin  $S_i = 2$  contribution to the capture reaction, and (c) that capture

to the  $1^+$  excited state of  $^8\text{Li}$  was not a prediction, but an input to constrain our EFT parameters. Point (c) was our choice and true in certain sense, though the best we can do within halo EFT itself: in [31] we fixed two remaining renormalization constants (after fixing the usual ones from scattering lengths and binding energies) to just two input data, the thermal neutron capture cross section to the ground  $2^+$  and first excited  $1^+$  states of  $^8\text{Li}$  [6], and postdict capture data at other energies. Zhang *et al.*, on the other hand, fix their remaining renormalization constants from their *ab initio* model. Answer to points (a) and (b) was the motivation of the present work.

We include the  $\frac{1}{2}^-$  excited state of  $^7\text{Li}$  core ( $^7\text{Li}^*$ ) as an explicit degree of freedom in a coupled-channel formalism, along similar lines of Refs. [33, 34]. In our formulation, the  $^7\text{Li}^*$  excited core influences only the channel with total spin  $S = 1$ , which is regarded as a subleading contribution. Our capture calculations show that the contributions from the excited core degree of freedom are negligible for momenta in the keV regime, and starts being noticeable only beyond the  $3^+$  resonant state of  $^8\text{Li}$ , albeit compatible with a typical next-to-next-to-leading (NNLO) correction. A power-counting is proposed that naturally incorporates the NLO contributions of the  $S = 1$  channel and  $^7\text{Li}^*$  excited core, the latter with kinematic imprints only at NNLO. We also compare our coupled-channel expressions and the respective low-energy expansions with those from Zhang *et al.* and comment on the discrepancies found.

The paper is organized as follows. In Sec. II we present the framework of halo EFT for two scenarios: without [30, 31] and with the  $^7\text{Li}^*$  excited core as an explicit degree of freedom, the latter with the pertinent channels that couple. There we highlight the differences between our and Zhang *et al.*'s formulations for the  $^7\text{Li}^*$  excited core in EFT. Section III contains the relevant formulas for the  $^7\text{Li}(n, \gamma)^8\text{Li}$  capture reaction in both theories with and without  $^7\text{Li}^*$ . A survey of possible families of EFT parameters compatible with given observables is discussed in Sec. IV, followed by the proposed power-counting in Sec. V. Numerical results and analyses are presented in Sec. VI with concluding remarks in Sec. VII.

## II. INTERACTION

In this section we construct two halo EFTs: one without the explicit  $^7\text{Li}^*$  degree of freedom that we refer to as just EFT and one with that we refer to as EFT $_{\star}$ . In the former, the low-energy degrees of freedom would be the spin-parity  $\frac{1}{2}^+$  neutron, the  $\frac{3}{2}^-$  ground state of  $^7\text{Li}$ , and the photon. In the latter we also have the  $\frac{1}{2}^-$  excited  $^7\text{Li}^*$  state as an additional degree of freedom. The  $2^+$  ground and  $1^+$  excited states of  $^8\text{Li}$  are represented as  $p$ -wave bound states of the neutron and the  $^7\text{Li}/^7\text{Li}^*$  core with binding momenta  $\gamma_0 \approx 57.78$  MeV and  $\gamma_1 \approx 41.56$  MeV, respectively [35]. We identify the relative center-of-mass (c.m.) momentum  $p$  and the binding energies with a low momentum scale  $Q \sim \gamma_1 \sim \gamma_0 \gtrsim p$ . The breakdown scale  $\Lambda \sim 150$  MeV is associated with pion physics,  $^4\text{He}$ - $^3\text{H}$  break up of the core, etc [30, 31]. The calculation is organized as an expansion in the small ratio  $Q/\Lambda \sim 1/3$ . We only consider the non-resonant E1 capture. The M1 contribution from the  $3^+$  resonance initial state has been considered in Ref. [31], and would be revisited in a future publication [36].

A radiative capture calculation requires a description of the initial scattering states, the final bound states, and the electroweak transition operators. The dominant contribution to capture at low momentum is from initial  $s$ -wave states to the final  $p$ -wave bound state through the E1 transition. The electroweak operators relevant to our calculation are one-

body currents produced through minimal substitution by gauging incoming momenta  $\mathbf{q} \rightarrow \mathbf{q} + eZ_c\mathbf{A}$  where  $Z_c = 3$  is the charge of the  ${}^7\text{Li}/{}^7\text{Li}^*$  core. Thus we start with a framework for the strong interaction that describes the initial scattering states, the final bound states, and the E1 operators.

The strong interaction in the first halo EFT is given by the Lagrangian

$$\begin{aligned} \mathcal{L} = & N^\dagger \left[ i\partial_0 + \frac{\nabla^2}{2m_n} \right] N + C^\dagger \left[ i\partial_0 + \frac{\nabla^2}{2m_c} \right] C + \chi_{[j]}^{(\zeta)\dagger} \left[ \Delta^{(\zeta)} + h^{(\zeta)} \left( i\partial_0 + \frac{\nabla^2}{2M} \right) \right] \chi_{[j]}^{(\zeta)} \\ & + \sqrt{\frac{2\pi}{\mu}} \left[ \chi_{[j]}^{(\zeta)\dagger} N^T P_{[j]}^{(\zeta)} C + \text{h.c.} \right], \end{aligned} \quad (1)$$

where  $N$  represents the  $\frac{1}{2}^+$  neutron with mass  $m_n = 939.6$  MeV,  $C$  represents the  $\frac{3}{2}^-$   ${}^7\text{Li}$  core with mass  $m_c = 6535.4$  MeV [37, 38],  $M = m_n + m_c$  is the total mass, and  $\mu = m_n m_c / M$  the reduced mass. We use natural units  $\hbar = 1 = c$ . The dimer fields  $\chi_{[j]}^{(\zeta)}$  are auxiliary that are introduced for convenience. Repeated indices are summed over. The neutron and  ${}^7\text{Li}$  core interact with each other through the exchange of the  $\chi_{[j]}^{(\zeta)}$  fields. These auxiliary fields can be integrated out of the theory to generate neutron-core contact interactions. The unknown couplings  $h^{(\zeta)}$  are included in the dimer propagator [39], for convenience, instead of an equivalent formulation where they appear in the dimer-particle interaction [30, 31].  $P_{[j]}^{(\zeta)}$  are the projectors for the relevant  $s$ - and  $p$ -wave channels in the spectroscopic notation  $2S+1L_J$ :  ${}^3S_1$ ,  ${}^5S_2$ ,  ${}^3P_1$ ,  ${}^3P_2$ ,  ${}^5P_1$ ,  ${}^5P_2$  [30, 31] indicated by the superscript  $\zeta$ . We provide their explicit form in Appendix A. The subscript  $[j]$  is a single index or double indices as appropriate for  $J = 1$  and  $J = 2$  states, respectively. For example, with  $\zeta = {}^3P_2$  one should read  $\chi_{[j]}^{(\zeta)} = \chi_{ij}^{({}^3P_2)}$  and  $P_{[j]}^{(\zeta)} = P_{ij}^{({}^3P_2)}$ . The couplings  $\Delta^{(\zeta)}$ ,  $h^{(\zeta)}$  can in principle be related to elastic scattering phase shifts if available. The E1 contribution to  ${}^7\text{Li}(n, \gamma){}^8\text{Li}$  has been calculated using this theory in Refs [30, 31]. We will present the results in Section III.

The second halo EFT with excited  ${}^7\text{Li}^*$  core (EFT $_\star$ ) can be described with the Lagrangian

$$\begin{aligned} \mathcal{L}_\star = & N^\dagger \left[ i\partial_0 + \frac{\nabla^2}{2m_n} \right] N + C^\dagger \left[ i\partial_0 + \frac{\nabla^2}{2m_c} \right] C + C_\star^\dagger \left[ i\partial_0 - E_\star + \frac{\nabla^2}{2m_c} \right] C_\star \\ & + \chi_{[j]}^{(\zeta')\dagger} \left[ \Pi^{(\zeta')} + t^{(\zeta')} \left( i\partial_0 + \frac{\nabla^2}{2M} \right) \right] \chi_{[j]}^{(\zeta')} \\ & + \sqrt{\frac{2\pi}{\mu}} \left[ \chi_{[j]}^{(\zeta)\dagger} N^T P_{[j]}^{(\zeta)} C + \chi_{[j]}^{(\zeta')\dagger} N^T P_{[j]}^{(\zeta')} C_\star + \text{h.c.} \right]. \end{aligned} \quad (2)$$

Here the  $C_\star$  field represents the excited  ${}^7\text{Li}^*$  core with excitation energy  $E_\star = 0.47761$  MeV [40]. There are a few other differences with the previous halo EFT without excited core in Eq. (1). In this theory, we have the additional scattering channels  ${}^3S_1^\star$ ,  ${}^3P_2^\star$ , and  ${}^3P_1^\star$  involving the  $C_\star$  field. We also allow for the possibility of mixing between channels which is induced by the off-diagonal terms in the dimer field  $\chi_{[j]}^{(\zeta)}$  (inverse) propagators. The couplings  $\Pi^{(\zeta')}$  and  $t^{(\zeta')}$  can again be related to scattering phase shifts if available. The generic index  $\zeta$  is used to represent all the channels, and one has to appropriately consider interactions only in the relevant channels as discussed below. We associate a low-momentum scale  $\gamma_\Delta = \sqrt{2\mu E_\star} \approx 28.0$  MeV  $\sim Q$  with the excited core [32].

We consider mixing in three pairs of channels:  ${}^3S_1$ - ${}^3S_1^\star$ ,  ${}^3P_1$ - ${}^3P_1^\star$  and  ${}^3P_2$ - ${}^3P_2^\star$ . However the formalism can be extended to other scattering channels as well. One could do the same to

include mixing between all  $S = 1$  and  $S = 2$   $p$ -wave channels. However, given that capture in the  $S = 2$  channel is 4 times that in the  $S = 1$  channel [41–43], any possible mixing between the different spin channels would be subleading, and beyond the order considered in this work.

### A. ${}^3S_1$ - ${}^3S_1^*$ Coupled-Channel

A coupled-channel calculation involving  $s$ -wave states was presented in Ref. [33]. See Ref. [34] as well for a coupled-channel calculation with and without Coulomb interaction for  $s$ -wave bound states. Here we present a slightly different derivation using the dimer fields instead of nucleon-core contact interactions. Some of the renormalization conditions are a little different but the final results expressed in terms of scattering parameters are the same.

The coupled-channel  $s$ -wave scattering amplitude is a  $2 \times 2$  matrix written as

$$i\mathcal{A}^{(ab)}(p) = -\frac{2\pi}{\mu} i\mathcal{D}^{(ab)}(E, 0), \quad (3)$$

where  $E = p^2/(2\mu)$  is the c.m. energy and the superscripts are the row-column indices of the amplitude matrix. We identify the  ${}^3S_1$  state as channel 1, and the  ${}^3S_1^*$  state as channel 2. The dimer propagator is given by the integral equation

$$\mathcal{D}(E, 0) = \mathcal{D}_0(E, 0) + \mathcal{D}_0(E, 0)\Sigma(E, 0)\mathcal{D}(E, 0), \quad (4)$$

which is conveniently calculated from its inverse

$$\mathcal{D}^{-1} = \mathcal{D}_0^{-1} - \Sigma, \quad (5)$$

where  $\mathcal{D}_0^{-1}$  is the inverse free dimer propagator and  $\Sigma$  is the self-energy. We have the free inverse dimer propagator directly from Eq. (2):

$$[\mathcal{D}_0(E, 0)]^{-1} = \begin{pmatrix} \Pi^{(11)} & \Pi^{(12)} \\ \Pi^{(12)} & \Pi^{(22)} \end{pmatrix}, \quad (6)$$

where we only kept the couplings  $\Pi^{(ij)}$  in a low-momentum expansion. In a single-channel calculation this would correspond to keeping only the scattering length contribution. The self-energy is

$$\begin{aligned} -\Sigma(E, 0) &= -\frac{2\pi}{\mu} \begin{pmatrix} J_0(\sqrt{-p^2 - i0^+}) & 0 \\ 0 & J_0(\sqrt{-p^2 + \gamma_\Delta^2 - i0^+}) \end{pmatrix}, \\ J_0(x) &= -2\mu \left(\frac{\lambda}{2}\right)^{4-D} \int \frac{d^{D-1}\mathbf{q}}{(2\pi)^{D-1}} \frac{1}{q^2 + x^2} = -\frac{\mu}{2\pi}(\lambda - x), \end{aligned} \quad (7)$$

where  $\lambda$  is the renormalization group (RG) scale. We use dimensional regularization in the so-called power divergence subtraction (PDS) scheme [44] that removes all divergences in space-time dimensions  $D \leq 4$ . The scattering amplitude has to be independent of  $\lambda$  which can be accomplished with the renormalized couplings

$$\Pi^{(ij)} = \frac{1}{a_{ij}} - \lambda\delta_{ij}, \quad (8)$$

where we introduced the scattering lengths  $a_{ij}$  following Ref. [33]. Then we get

$$[\mathcal{D}(E, 0)]^{-1} = \begin{pmatrix} \frac{1}{a_{11}} + ip & \frac{1}{a_{12}} \\ \frac{1}{a_{12}} & \frac{1}{a_{22}} - \sqrt{-p^2 + \gamma_\Delta^2 - i0^+} \end{pmatrix}, \quad (9)$$

and in particular the  $s$ -wave amplitude

$$\mathcal{A}^{(11)}(p) = \frac{2\pi}{\mu} \frac{-\frac{1}{a_{22}} + \sqrt{-p^2 + \gamma_\Delta^2 - i0^+}}{(-\frac{1}{a_{11}} - ip)(-\frac{1}{a_{22}} + \sqrt{-p^2 + \gamma_\Delta^2 - i0^+}) - \frac{1}{a_{12}^2}}, \quad (10)$$

which reduces to the single-channel amplitude when the mixing coupling  $\Delta_{12} = 1/a_{12}$  is set to zero. The off-diagonal amplitude mixing channels 1 and 2 is

$$\mathcal{A}^{(12)}(p) = \frac{2\pi}{\mu} \frac{1/a_{12}}{(-\frac{1}{a_{11}} - ip)(-\frac{1}{a_{22}} + \sqrt{-p^2 + \gamma_\Delta^2 - i0^+}) - \frac{1}{a_{12}^2}}. \quad (11)$$

These expressions agree with Eq. (2.19) from Ref. [33].

At momenta  $p \ll \gamma_\Delta$ , the scattering amplitudes should be analytic around  $p = 0$ , and in particular  $\mathcal{A}^{(11)}$  should be given by the effective range expansion (ERE). So we need

$$\begin{aligned} -\frac{1}{a_{11}} - a_{12}^{-2}/(-\frac{1}{a_{22}} + \sqrt{-p^2 + \gamma_\Delta^2 - i0^+}) &\approx -\frac{1}{a_{11}} + \frac{a_{22}a_{12}^{-2}}{1 - a_{22}\gamma_\Delta} - \frac{1}{2} \frac{a_{22}^2a_{12}^{-2}}{\gamma_\Delta(1 - a_{22}\gamma_\Delta)^2} p^2 + \dots \\ &= -\frac{1}{a_0^{(1)}} + \frac{1}{2} r_0^{(1)} p^2 + \dots, \end{aligned} \quad (12)$$

where  $a_0^{(1)}$  and  $r_0^{(1)}$  are the scattering length and effective range in the  $^3S_1$  channel, respectively. Matching the EFT expression to the ERE one obtains

$$\begin{aligned} a_{11} &= a_0^{(1)} \frac{1 - a_{22}\gamma_\Delta}{1 + a_{22}(a_0^{(1)}a_{12}^{-2} - \gamma_\Delta)}, \\ a_{12}^{-2} &= -r_0^{(1)}\gamma_\Delta \frac{(1 - a_{22}\gamma_\Delta)^2}{a_{22}^2}. \end{aligned} \quad (13)$$

We can fix  $a_{11}$  from  $a_0^{(1)}$  and  $a_{12}$  from  $r_0^{(1)}$ , leaving  $a_{22}$  as an undetermined parameter which could in principle be obtained from the low-momentum measurement of  $\mathcal{A}^{(12)}$  [45]. One should note that in the halo EFT<sub>★</sub> with  $^7\text{Li}^*$ , an effective range  $r_0^{(1)}$  is generated dynamically though we started with a momentum-independent interaction because there is a momentum associated with the excitation energy of the core. Ref. [33] considered the situation where the scattering lengths  $a_{ij} \sim 1/Q$  are fine-tuned. Then it produces a fine-tuned negative effective range  $|r_0^{(1)}| \sim 1/Q$  as well for  $\gamma_\Delta \sim Q$ . In the  $^8\text{Li}$  system  $a_0^{(1)} = 0.87(7)$  fm [46] which is of natural size  $1/\Lambda$ . Thus we assume that all the scattering lengths  $a_{ij} \sim 1/\Lambda$  are of natural size as well which still produces a fine-tuned negative effective range  $|r_0^{(1)}| \sim 1/Q$ .

Then we can expand in the  $Q/\Lambda$  ratio and write

$$\begin{aligned}
\mathcal{A}^{(11)}(p) &= \frac{2\pi}{\mu} \frac{1}{-\frac{1}{a_0^{(1)}} + r_0^{(1)} \gamma_\Delta \frac{1-a_{22}\gamma_\Delta}{a_{22}} - r_0^{(1)} \gamma_\Delta \frac{(1-a_{22}\gamma_\Delta)^2}{a_{22}(1-a_{22}\sqrt{-p^2+\gamma_\Delta^2-i0^+})} - ip} \\
&\approx -\frac{2\pi}{\mu} a_0^{(1)} \left[ 1 - ia_0^{(1)} p + a_0^{(1)} r_0^{(1)} \gamma_\Delta^2 - a_0^{(1)} r_0^{(1)} \gamma_\Delta \sqrt{-p^2 + \gamma_\Delta^2 - i0^+} + \dots \right], \\
\mathcal{A}^{(12)}(p) &= \frac{2\pi}{\mu} a_0^{(1)} \sqrt{-r_0^{(1)} \gamma_\Delta (1/a_{22} - \gamma_\Delta)^2} \times \left[ \frac{1}{a_{22}} - \sqrt{-p^2 + \gamma_\Delta^2 - i0^+} \right. \\
&\quad \left. - a_0^{(1)} r_0^{(1)} \gamma_\Delta \left( \frac{1}{a_{22}} - \gamma_\Delta \right) (\gamma_\Delta - \sqrt{-p^2 + \gamma_\Delta^2 - i0^+}) \right. \\
&\quad \left. + ia_0^{(1)} p \left( \frac{1}{a_{22}} - \sqrt{-p^2 + \gamma_\Delta^2 - i0^+} \right) \right]^{-1} \\
&\approx \frac{2\pi}{\mu} a_0^{(1)} a_{22} \sqrt{\frac{-r_0^{(1)} \gamma_\Delta}{a_{22}^2}} \left[ 1 - ia_0^{(1)} p + \left( \gamma_\Delta - \sqrt{-p^2 + \gamma_\Delta^2 - i0^+} \right) \right. \\
&\quad \left. \times \left( a_0^{(1)} r_0^{(1)} \gamma_\Delta - a_{22} \right) + \dots \right]. \tag{14}
\end{aligned}$$

The  $Q/\Lambda$  expansion in Eq. (14) implies that the non-analyticity from the open channel involving the excited core  ${}^7\text{Li}^*$  is a subleading effect.

## B. ${}^3P_2$ - ${}^3P_2^*$ Coupled-Channel

The coupled-channel calculation for  $p$ -wave states is very similar to the  $s$ -wave states in subsection II A. An important difference is that for  $p$ -waves we need effective momentum corrections at LO [25, 26]. Now we write the free inverse dimer propagator as

$$[\mathcal{D}_0(E, 0)]^{-1} = \begin{pmatrix} \Pi^{(11)} + Et^{(11)} & \Pi^{(12)} + Et^{(12)} \\ \Pi^{(12)} + Et^{(12)} & \Pi^{(22)} + Et^{(22)} \end{pmatrix}, \tag{15}$$

where we identify  ${}^3P_1$  as channel 1 and  ${}^3P_1^*$  as channel 2. The  $p$ -wave self-energy term is given by

$$\begin{aligned}
-\Sigma(E, 0) &= -\frac{6\pi}{\mu^3} \begin{pmatrix} J_1(\sqrt{-p^2 - i0^+}) & 0 \\ 0 & J_1(\sqrt{-p^2 + \gamma_\Delta^2 - i0^+}) \end{pmatrix}, \\
J_1(x) &= -\frac{2\mu}{D-1} \left( \frac{\lambda}{2} \right)^{4-D} \int \frac{d^{D-1}\mathbf{q}}{(2\pi)^{D-1}} \frac{q^2}{q^2 + x^2} = -\frac{\mu}{6\pi} \left( x^3 - \frac{3}{2}x^2\lambda + \frac{\pi}{2}\lambda^3 \right). \tag{16}
\end{aligned}$$

The RG conditions (no sum over repeated indices intended)

$$\begin{aligned}
\mu^2 \Pi^{(ij)} &= \frac{1}{a_{ij}} - \frac{\pi}{2} \lambda^3 \delta_{ij} + \frac{3}{2} \gamma_\Delta^2 \lambda \delta_{i2} \delta_{ij}, \\
\mu^2 t^{(ij)} &= -\mu(r_{ij} + 3\lambda \delta_{ij}), \tag{17}
\end{aligned}$$

make the inverse propagator (and the scattering amplitude)  $\lambda$ -independent:

$$[\mathcal{D}(E, 0)]^{-1} = \frac{1}{\mu^2} \begin{pmatrix} \frac{1}{a_{11}} - \frac{1}{2}r_{11}p^2 + ip^3 & \frac{1}{a_{12}} - \frac{1}{2}r_{12}p^2 \\ \frac{1}{a_{12}} - \frac{1}{2}r_{12}p^2 & \frac{1}{a_{22}} - \frac{1}{2}r_{22}p^2 + (-p^2 + \gamma_\Delta^2 - i0^+)^{3/2} \end{pmatrix}, \tag{18}$$

where  $a_{ij}$  are the  $p$ -wave scattering volumes, and  $r_{ij}$  the  $p$ -wave effective momenta. The  $p$ -wave coupled-channel amplitude is given by

$$\mathcal{A}(p) = -\frac{2\pi}{\mu} \frac{p^2}{\mu^2} \mathcal{D}(E, 0). \quad (19)$$

The wave function renormalization constant that enters the capture calculation is

$$\begin{aligned} [\mathcal{Z}]^{-1} &= \frac{d}{dE} [\mathcal{D}(E, 0)]^{-1} \Big|_{E=-B} = -\frac{1}{\mu} \begin{pmatrix} r_{11} + 3\gamma & r_{12} \\ r_{12} & r_{22} + 3\sqrt{\gamma^2 + \gamma_\Delta^2} \end{pmatrix}, \\ \frac{2\pi}{\mu} \mathcal{Z} &= -2\pi \begin{pmatrix} \frac{3\sqrt{\gamma^2 + \gamma_\Delta^2} + r_{22}}{(3\gamma + r_{11})(3\sqrt{\gamma^2 + \gamma_\Delta^2} + r_{22}) - r_{12}^2} & \frac{-r_{12}}{(3\gamma + r_{11})(3\sqrt{\gamma^2 + \gamma_\Delta^2} + r_{22}) - r_{12}^2} \\ \frac{-r_{12}}{(3\gamma + r_{11})(3\sqrt{\gamma^2 + \gamma_\Delta^2} + r_{22}) - r_{12}^2} & \frac{3\gamma + r_{11}}{(3\gamma + r_{11})(3\sqrt{\gamma^2 + \gamma_\Delta^2} + r_{22}) - r_{12}^2} \end{pmatrix}, \end{aligned} \quad (20)$$

with binding momentum  $\gamma = \sqrt{2\mu B}$ . The wave function renormalization constant reduces to the single-channel result [30, 31] when  $r_{12}$  vanishes. In our calculation we will not assume  $r_{12}$  to be small. We will simply fit the constants  $\mathcal{Z}_{11}$ ,  $\mathcal{Z}_{12}$  to the ANCs without attempting to interpret what it implies in terms of the scattering parameters because the two  ${}^3P_1$ ,  ${}^3P_1^*$  ANCs are not sufficient to determine the three effective momenta  $r_{ij}$ . The coupled-channel  ${}^3P_2$ - ${}^3P_2^*$  calculation is very similar.

The calculation by Zhang *et al.* [32] differs from our result for the  ${}^7\text{Li}^*$  contribution in several manners. In the  $s$ -wave initial states, Ref. [32] uses a very specific interaction where the scattering amplitude  $\mathcal{A}^{(12)}$  in the inelastic channel  ${}^3S_1$ - ${}^3S_1^*$  is assumed to be determined once the amplitudes  $\mathcal{A}^{(11)}$  and  $\mathcal{A}^{(22)}$  are given. In particular, they use a single dimer field that couples to the  ${}^3S_1$  and  ${}^3S_1^*$  states with two different couplings. By construction, their theory uses two couplings to describe the coupled-channel calculation. When the auxiliary dimer field is integrated out of the field theory, it will generate neutron-core contact interactions where the  ${}^3S_1$ - ${}^3S_1^*$  coupling is simply the geometric mean of the couplings in the  ${}^3S_1$  and  ${}^3S_1^*$  channels. Accordingly, their corresponding scattering length  $a_{12}$  is not a free parameter but given by  $a_{11}$ , and  $a_{22}$ . The coupled-channel calculations presented here and in Refs. [33, 34], in contrast, require three renormalized couplings at LO that depend on three independent scattering lengths  $a_{11}$ ,  $a_{12}$ , and  $a_{22}$ . *A priori* there is no expectation that  $a_{12}$  is a function of  $a_{11}$  and  $a_{22}$ .

In the final  $p$ -wave  $2^+$  ground state calculation, the interaction used by Zhang *et al.* [32] produces mixing between all  $p$ -wave channels:  ${}^5P_2$ ,  ${}^3P_2$  and  ${}^3P_2^*$ , see Eq. (14) in Ref. [32]. The interaction they use is such that the amplitudes in the inelastic channels are specified once the elastic channels are known. The wave function renormalization constant is written in terms of a single  $p$ -wave effective momentum. However, we note that the renormalization condition imposed in deriving Eq. (15) of Ref. [32] for the wave function renormalization constant ignores the contribution from the mixing between  ${}^5P_2$ - ${}^3P_2$  that is present in their formulation. This would affect their result. In contrast, we consider only a coupled-channel calculation in  ${}^3P_2$ - ${}^3P_2^*$  for the  $2^+$  ground state of  ${}^8\text{Li}$ . The coupled-channel  $p$ -wave amplitudes depend on three scattering volumes  $a_{ij}$  and three effective momenta  $r_{ij}$ . The associated wave function renormalization constant depends on the three effective momenta  $r_{ij}$ . A coupled-channel calculation mixing three channels in general would involve 6 effective momenta for the wave function renormalization, and not one effective momentum as suggested [32]. In the EFT without explicit  ${}^7\text{Li}^*$  core, the  ${}^5P_2$  and  ${}^3P_2$  channels do not mix and we require two independent effective momenta [30, 31]. There are some other minor technical differences in



our calculations such that we subtract both the linear and cubic divergences for the  $p$ -waves in PDS [30, 31] instead of just the linear divergences [32].

### III. CAPTURE CALCULATION

The E1 capture reaction  ${}^7\text{Li}(n, \gamma){}^8\text{Li}$  is given by the diagrams in Fig. 1. Capture in the  $S = 2$  channel dominates and in our formulation it doesn't mix with the  $S = 1$  channel. The excited core  ${}^7\text{Li}^*$  contributes only in the  $S = 1$  channel. Thus the  $S = 2$  channel calculation in both EFT and EFT $_{\star}$  are very similar.

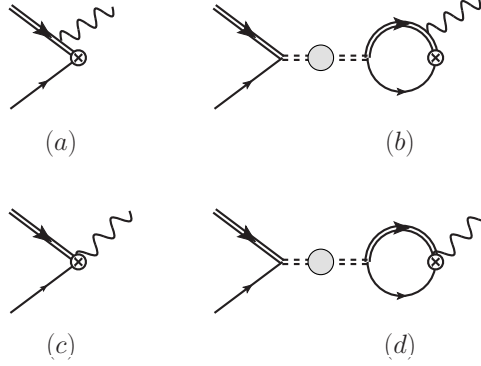


FIG. 1. Double solid line represents a  ${}^7\text{Li}$  or  ${}^7\text{Li}^*$  core as appropriate, single solid line a neutron, double dashed line a dressed dimer propagator, wavy line a photon, and  $\otimes$  represents the final bound state.

We start with the calculation in the  $S = 2$  channel in EFT without  ${}^7\text{Li}^*$  first. The squared amplitude for the capture from the initial  ${}^5S_2$  state to the  $2^+$  ground state  ${}^8\text{Li}$  is [30, 31]

$$\begin{aligned} \left| \mathcal{M}_{\text{E1}}^{(5P_2)} \right|^2 &= (2j+1) \left( \frac{Z_c m_n}{M} \right)^2 \frac{64\pi\alpha M^2}{\mu} \frac{2\pi}{\mu} \mathcal{Z}^{(5P_2)} \\ &\times \left| 1 - \frac{2}{3} \frac{p^2}{p^2 + \gamma_0^2} - \mathcal{A}_0(a_0^{(2)}, p) [B_0(p, \gamma_0) + J_0(-ip)] \right|^2, \end{aligned} \quad (21)$$

where  $j = 2$ . The initial state strong interaction in the  $s$ -wave is given by the amplitude

$$\mathcal{A}_0(a_0^{(2)}, p) = \frac{2\pi}{\mu} \frac{1}{-\frac{1}{a_0^{(2)}} - ip}, \quad (22)$$

with the scattering length  $a_0^{(2)} = -3.63(5) \text{ fm}$  [46] scaling as  $1/Q$ . The loop contribution from diagram (b) of Fig. 1 is contained in the function

$$\begin{aligned} B_0(p, \gamma) &= \frac{4\mu}{D-1} \left( \frac{\lambda}{2} \right)^{4-D} \int \frac{d^{D-1}\mathbf{q}}{(2\pi)^{D-1}} \frac{q^2}{(q^2 - p^2 - i0^+)(q^2 + \gamma^2)} \\ &= \mu \left( \frac{\lambda}{2\pi} + \frac{1}{3\pi} \frac{ip^3 - \gamma^3}{p^2 + \gamma^2} \right). \end{aligned} \quad (23)$$

Fig. 1 (d) is proportional to  $J_0(-ip)$ . The combination  $B_0(p, \gamma) + J_0(-ip)$  is RG scale independent. The wave function renormalization constant in the  ${}^5P_2$  channel has the simple form

$$\frac{2\pi}{\mu} \mathcal{Z}^{({}^5P_2)} = -\frac{2\pi}{r_1^{({}^5P_2)} + 3\gamma_0}, \quad (24)$$

where  $r_1^{({}^5P_2)}$  is the  $p$ -wave effective momentum in the  ${}^5P_2$  channel. In this EFT without explicit  ${}^7\text{Li}^*$ , the capture from initial  ${}^3S_1$  state to the  $2^+$  ground state is given by a similar expression as above in Eq. (21) with the replacements  $a_0^{(2)} \rightarrow a_0^{(1)}$  for the scattering length in the  ${}^3S_1$  channel, and  $r_1^{({}^5P_2)} \rightarrow r_1^{({}^3P_2)}$  for the effective momentum in the  ${}^3P_2$  channel.

It is straightforward to extend this EFT calculation for the capture to the  $1^+$  excited state—one replaces  $j = 1$  in Eq. (21),  $\gamma_0 \rightarrow \gamma_1$  for the  $1^+$  state binding momentum, and uses the appropriate  $p$ -wave effective momenta in the  ${}^3P_1$  and  ${}^5P_1$  final states.

Next we discuss the capture process in  $\text{EFT}_\star$  that contains explicit  ${}^7\text{Li}^*$  core contributions. The capture in the spin  $S = 2$  remains exactly the same as Eq. (21). The additional contributions in  $\text{EFT}_\star$  come from Figs. 1 (b) and (d) in the spin  $S = 1$  where the initial state  $s$ -wave interactions have to be described in terms of coupled-channel amplitudes  $\mathcal{A}^{(11)}$  and  $\mathcal{A}^{(12)}$  derived earlier in Eq. (14). The contribution from  $\mathcal{A}^{(12)}$  also entails modifying the momentum of the core in the loops with a photon attached in Fig. 1 (b) and (d). A direct calculation of capture to the  $2^+$  ground state in spin  $S = 1$  channel is then given by

$$\begin{aligned} \left| \mathcal{M}_{\text{E1},\star}^{({}^3P_2)} \right|^2 &= (2j+1) \left( \frac{Z_c m_n}{M} \right)^2 \frac{64\pi\alpha M^2}{\mu} \frac{2\pi}{\mu} \mathcal{Z}^{({}^3P_2)} \\ &\times \left| 1 - \frac{2}{3} \frac{p^2}{p^2 + \gamma^2} - \mathcal{A}^{(11)}(p) [B_0(p, \gamma) + J_0(-ip)] \right. \\ &\quad \left. - \mathcal{A}^{(12)}(p) \left[ B_0 \left( i\sqrt{-p^2 + \gamma_\Delta^2} - i0^+, \sqrt{\gamma_0^2 + \gamma_\Delta^2} \right) \right. \right. \\ &\quad \left. \left. + J_0 \left( \sqrt{-p^2 + \gamma_\Delta^2} - i0^+ \right) \right] \frac{\sqrt{\mathcal{Z}^{({}^3P_2^*)}}}{\sqrt{\mathcal{Z}^{({}^3P_2)}}} \right|^2. \end{aligned} \quad (25)$$

The extension to the capture to the  $1^+$  state with  $j = 1$  is straightforward with  $\gamma_0 \rightarrow \gamma_1$  and the appropriate modification of the wave function renormalization constants  $\mathcal{Z}^{({}^3P_2)} \rightarrow \mathcal{Z}^{({}^3P_1)}$ ,  $\mathcal{Z}^{({}^3P_2^*)} \rightarrow \mathcal{Z}^{({}^3P_1^*)}$  for the  ${}^3P_1$  and  ${}^3P_1^*$  states, respectively.

The total c.m. cross section for the capture to the  $2^+$  state is given by

$$\sigma_{\text{E1}}^{(2+)}(p) = \frac{1}{16\pi M^2} \frac{k_0}{p} \frac{1}{8} \left[ |a|^2 \left| \mathcal{M}_{\text{E1}}^{({}^5P_2)} \right|^2 + (1 - |a|^2) \left| \mathcal{M}_{\text{E1}}^{({}^3P_2)} \right|^2 \right], \quad (26)$$

in the EFT without excited  ${}^7\text{Li}^*$  core and by

$$\sigma_{\text{E1},\star}^{(2+)}(p) = \frac{1}{16\pi M^2} \frac{k_0}{p} \frac{1}{8} \left[ |a|^2 \left| \mathcal{M}_{\text{E1}}^{({}^5P_2)} \right|^2 + (1 - |a|^2) \left| \mathcal{M}_{\text{E1},\star}^{({}^3P_2)} \right|^2 \right], \quad (27)$$

in the  $\text{EFT}_\star$  with  ${}^7\text{Li}^*$  core as explicit degree of freedom. We use the normalized bound state

$$|2^+, m\rangle = a|S = 2, L = 1, J = 2, m\rangle + \sqrt{1 - |a|^2} |S = 1, L = 1, J = 2, m\rangle, \quad (28)$$

in both EFT and EFT<sub>\*</sub>. The choice  $a = 1/\sqrt{2}$ , makes  $|2^+\rangle$  a  $p_{3/2}$  valance neutron state that we use in this work [8, 24]. The mixing with the  $|^3P_2^*\rangle$  state in the coupled-channel calculation is included through the interaction. One views the relation in Eq. (28) above as an interpolating field that only needs to have the correct quantum numbers of the ground state. The details of the ground state are built in through the interaction in the theory, such as by the factors of  $\mathcal{Z}(^3P_2^*)/\mathcal{Z}(^3P_2)$  in Eq. (25). The capture cross section to the  $1^+$  state of  $^8\text{Li}$  is similar with the appropriate change of parameters as detailed earlier. We take

$$|1^+, m\rangle = b|S = 2, L = 1, J = 1, m\rangle - \sqrt{1 - |b|^2}|S = 1, L = 1, J = 1, m\rangle, \quad (29)$$

with  $b = \sqrt{5/6}$ , making it a  $p_{1/2}$  valance neutron configuration [8, 24]. The choice  $b = 1/\sqrt{2}$  in Ref. [31] was an error that we correct here.

#### IV. A SURVEY

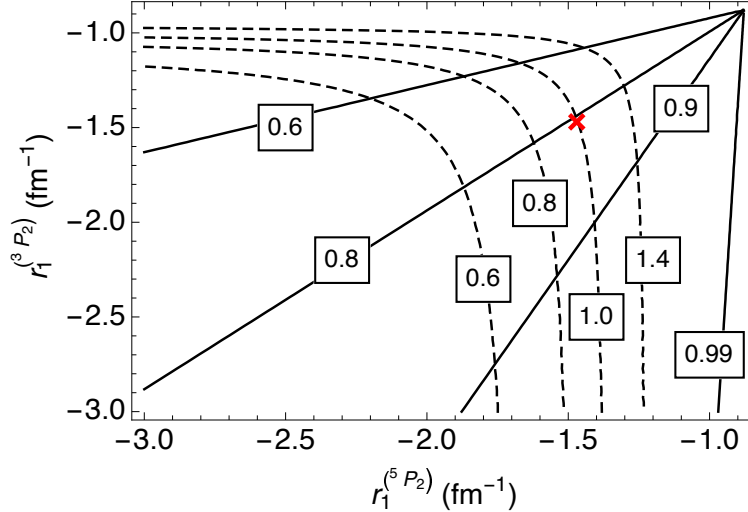


FIG. 2. EFT without  $^7\text{Li}^*$ . Dashed curves: Contour plot of capture cross section to the  $2^+$  state at thermal energy normalized to data [6]. Solid curves: Contour plot of branching ratio of capture cross section to the  $2^+$  state in the spin  $S = 2$  channel at thermal energy. The  $\times$  marks the parameter value  $r_1^{(^5P_2)} = -1.47 \text{ fm}^{-1} = r_1^{(^3P_2)}$  used in Ref. [31]. The boxed numbers indicate the values on the corresponding contour lines.

The E1 cross section in Eq. (26) was calculated earlier in Refs. [30, 31]. It depends on four scattering parameters  $a_0^{(2)}$ ,  $a_0^{(1)}$ ,  $r_1^{(^5P_2)}$  and  $r_1^{(^3P_2)}$ . The two effective momenta are not known experimentally, and the capture to the  $2^+$   $^8\text{Li}$  ground state is sensitive to only a combination of these. In the following we define the thermal ratio as the theory calculation of the capture cross section to the  $2^+$   $^8\text{Li}$  ground state at thermal energy, divided by the corresponding experimental value [6]. Fig. 2 shows that a single parameter family of  $p$ -wave effective momenta can reproduce a given thermal ratio (dashed curves). The solid curves show how a single parameter family of  $p$ -wave effective momenta can produce a given branching ratio of the capture to the  $S = 2$  channel at thermal energy. In Refs. [30, 31] a common

effective momentum  $r_1^{(2^+)} \sim \Lambda$  was used for both  $r_1^{(5P_2)}$  and  $r_1^{(3P_2)}$  for convenience which reproduced the thermal capture rate. This also gave a branching ratio that is consistent with the experimental lower bound of  $W_+ \geq 0.86$  [43], once the theory errors from the EFT in Ref. [31] are also taken into consideration. We mention that earlier works have estimated the lower bound as 0.80 [42] and 0.75 [41], respectively. Applying the branching ratio lower bound  $W_+ \geq 0.86$  to the experimental constraint on thermal capture cross section would restrict  $r_1^{(5P_2)} \sim -1.5 \text{ fm}^{-1}$  but leave  $r_1^{(3P_2)} \lesssim -2 \text{ fm}^{-1}$  completely unbound from below.

The result from Ref. [31], without initial state  $d$ -wave contribution, is plotted as EFT A in Fig. 3, where data from Refs.[6, 7, 9] are also shown. As pointed out in Ref. [32], one could use the known ANCs  $C_{1,\zeta}^2$  to fit the effective momenta using the relation:

$$C_{1,\zeta}^2 = \frac{\gamma^2}{\pi} \frac{2\pi}{\mu} \mathcal{Z}^{(\zeta)}, \quad (30)$$

where  $\gamma$  is the appropriate binding momentum in the channel  $\zeta$ . We use the following ANC values:  $C_{1,5P_2}^2 = 0.352(28) \text{ fm}^{-1}$ ,  $C_{1,3P_2}^2 = 0.080(13) \text{ fm}^{-1}$ ,  $C_{1,5P_1}^2 = 0.047(4) \text{ fm}^{-1}$ ,  $C_{1,3P_1}^2 = 0.035(5) \text{ fm}^{-1}$  from neutron transfer reaction [47] and  $C_{1,3P_2^*}^2 = 0.147(5) \text{ fm}^{-1}$ ,  $C_{1,3P_1^*}^2 = 0.0458(10) \text{ fm}^{-1}$  from an ab initio calculation [32].

The experimental ANCs from Ref. [47] give  $r_1^{(5P_2)} \sim -1.37 \text{ fm}^{-1}$ ,  $r_1^{(3P_2)} \sim -3.0 \text{ fm}^{-1}$  which are consistent with the expectation from the analysis of Fig. 2. The corresponding result for the capture cross section is plotted as EFT ANC in Fig. 3. Though the curves EFT A and EFT ANC differ, this difference is within the expected theoretical error. We provide a more robust theory error estimate later in Section V when we develop the EFT power counting relevant to E1 transition at low momenta. Table I lists some of the fit parameters, and the thermal and branching ratios.

In Fig. 3 we also plot the capture calculation to the  $2^+$  state in EFT $_{\star}$  with the explicit  ${}^7\text{Li}^{\star}$  degree of freedom. It is labeled as EFT $_{\star}$  ANC. In the spin  $S = 2$  channel this cross section depends on  $a_0^{(2)}$  and  $r_1^{(5P_2)}$ . In the  $S = 1$  channel we need the parameters  $a_0^{(1)}$ ,  $a_{12}$ ,  $a_{22}$ , and overall normalization constants  $\mathcal{Z}^{(3P_2)}$ ,  $\mathcal{Z}^{(3P_2^*)}$ . The unknowns  $r_1^{(5P_2)}$ ,  $\mathcal{Z}^{(3P_2)}$  are constrained from the experimental ANCs [47], and  $\mathcal{Z}^{(3P_2^*)}$  is constrained from the calculated ANC [32]. We take  $a_{22} = -1/200(1 \pm 0.4) \text{ MeV}^{-1}$  and get  $a_{12}$  from Eq. (13) with  $r_0^{(1)} = -6(1 \pm 0.4) \text{ fm}$ . We saw earlier in Eq. (13) that  $r_0^{(1)}$  is negative and fine-tuned to be large. A negative  $a_{22}$  appear to give a better description of data but this is not very crucial for the analysis. Using  $a_{22} = 1/200(1 \pm 0.4) \text{ MeV}^{-1}$  changes the cross section by a few percent (well within a NNLO contribution we discuss later). In this plot we did not approximate the  $s$ -wave scattering amplitudes  $\mathcal{A}^{(11)}$ ,  $\mathcal{A}^{(12)}$  in Eq. (14) by the  $Q/\Lambda$  expansion. One notices that the curves EFT ANC and EFT $_{\star}$  ANC are compatible with each other within the expected errors regarding their momentum dependence. In particular, the opening of the inelastic threshold at  $p = \gamma_{\Delta} = 28.0 \text{ MeV}$  remains a small effect. Nevertheless, the range of momentum where the explicit  ${}^7\text{Li}_{\star}$  degree of freedom gives the largest contributions is where the M1 capture due to the  $3^+$  resonance is already predominant [31]. Given that  $p_R < \gamma_{\Delta}$ , the inclusion of the  $3^+$  degree of freedom precedes that of the  ${}^7\text{Li}_{\star}$  in the formulation of the low-energy effective theory for the  ${}^7\text{Li}(n, \gamma){}^8\text{Li}$  reaction if we attempt to describe data. Nevertheless, one can analyze the non-resonant capture theoretically. We interpret the plot EFT $_{\star}$  ANC as indicative of the fact that the  ${}^7\text{Li}^{\star}$  contribution to the initial  $s$ -wave scattering at these energies is a subleading effect. The contribution of the  ${}^7\text{Li}^{\star}$  to the bound state wave function cannot be separated completely with the two ANCs for  ${}^3P_2$  and  ${}^3P_2^*$  states to constrain the

three relevant  $p$ -wave effective momenta  $r_{11}$ ,  $r_{12}$ , and  $r_{22}$  in Eq. (20). In Table I, we list the  $r_1^{(5P_2)}$  value, and the thermal and branching ratios for the EFT $_{\star}$  ANC fit.

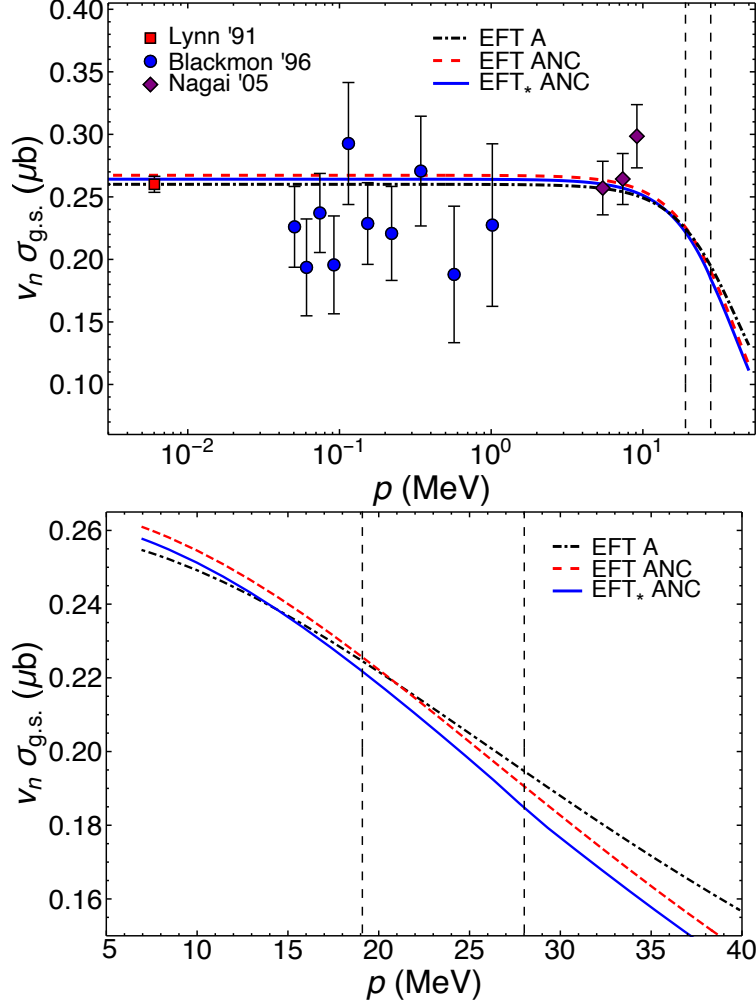


FIG. 3. Capture cross section to the  $2^+$  state  $\sigma_{\text{g.s.}}$  scaled by the neutron c.m. velocity  $v_n$  vs c.m. relative momentum  $p$ . The (black) dot-dashed curve is the EFT A result, the (red) dashed curve is the EFT ANC result, and the (blue) solid curve is the EFT $_{\star}$  ANC result, respectively. The grid lines are at the  $3^+$  resonance momentum  $p_R = 19.1$  MeV and the  ${}^7\text{Li}^*$  inelasticity  $\gamma_{\Delta} = 28.0$  MeV. The different curves are explained in the text.

## V. EFT AND EFT $_{\star}$ POWER COUNTING

We start with the capture to the dominant  $2^+$  state. Capture in the spin  $S = 2$  channel is about a factor of 4 larger than in the spin  $S = 1$  channel [48]. Thus we count capture in the  $S = 1$  channel to be NLO (a subleading effect). In the dominant spin channel, the  $s$ -wave scattering length  $a_0^{(2)} \sim 1/Q$  is large. At low momentum the contribution from the initial state interaction scales as  $a_0^{(2)}(B_0 + J_0)$ . The loop integral combination scales as

TABLE I.  ${}^7\text{Li}(n, \gamma){}^8\text{Li}$  capture to the  $2^+$  state. We estimate the parameters as described in the text. Thermal ratio is the EFT cross section normalized to Lynn data [6]. Branching ratio is the capture in the  $S = 2$  spin channel compared to the total cross section at thermal momentum. We show results to 3 significant figures.

Theory	$r_1^{(5P_2)}$ (fm $^{-1}$ )	$\mathcal{Z}^{(5P_2)}$	$\mathcal{Z}^{(3P_2)}$	Thermal ratio	Branching ratio
EFT A	-1.47(1)	7.08(17)	7.08(17)	1	0.809(9)
EFT ANC	-1.37(4)	8.54(68)	1.95(33)	1.03(8)	0.949(10)
EFT $_{\star}$ ANC	-1.37(4)	8.54(68)	1.95(33)	1.02(8)	0.960(11)
EFT/EFT $_{\star}$ Lynn LO	-0.476(12)	8.75(22)	—	1	1
EFT/EFT $_{\star}$ Lynn-ANC NLO	-1.39(1)	8.12(22)	1.85(34)	1	0.788(56)
EFT/EFT $_{\star}$ ANC LO	-0.488(39)	8.54(68)	—	0.975(79)	1
EFT/EFT $_{\star}$ ANC NLO	-1.37(4)	8.54(68)	1.95(33)	1.05(8)	0.781(55)

$B_0 + J_0 \sim Q$ . Thus the contributions from the diagrams with and those without initial state strong interactions in Fig. 1 are of the same size  $\mathcal{O}(1)$  in the  $Q/\Lambda$  expansion. This constitutes the LO contribution in both the EFT $_{\star}$  with  ${}^7\text{Li}^*$  and the EFT without.

The cross section in the  $S = 2$  channel is proportional to the wave function renormalization constant  $\mathcal{Z}^{(5P_2)}$  that depends on the effective momentum  $r_1^{(5P_2)} \sim \Lambda$  and binding momentum  $\gamma_0 \sim Q$ . Discounting factors of 3, we can expand  $\mathcal{Z}^{(5P_2)}$  in powers of  $Q/\Lambda$ . Here we use the so-called zed-parameterization introduced in Ref. [49] for  $s$ -wave bound states that can also be applied to  $p$ -wave bound states [31]. A consequence of this parameterization is that the wave function renormalization constant is exact at NLO with no other higher-order corrections but there is a substantial change in the parameters from LO to NLO, see  $r_1^{(5P_2)}$  values at LO and NLO in Table I. At NLO, there is an  $s$ -wave effective range  $r_0^{(2)} \sim 1/\Lambda$  correction. The capture data at low energy is not sensitive to this parameter. Fig. 4 shows the sensitivity to  $r_0^{(2)}$  in the range  $-5$  fm to  $5$  fm. We include this in our error estimates later in the analysis.

The capture in the spin  $S = 1$  channel starts at NLO, and the power counting for the EFT $_{\star}$  with  ${}^7\text{Li}^*$  and EFT without has to be discussed separately though they are the same up to NLO. We start with the theory without the excited  ${}^7\text{Li}^*$  core. In this theory, the contributions from Figs. 1 (b), (d) from the initial state interactions scale as  $a_0^{(1)}(B_0 + J_0)$ . Given the smaller  $a_0^{(1)} \sim 1/\Lambda$  in this channel, these initial state interactions are  $Q/\Lambda$  suppressed compared to the contributions from Figs. 1 (a), (c), thus they constitute a NNLO contribution. The wave function renormalization constant  $\mathcal{Z}^{(3P_2)}$  has the same form as Eq. (24) for the  $S = 2$  channel. Here we again use the zed-parameterization.

In EFT $_{\star}$  with explicit  ${}^7\text{Li}^*$  core contribution there are two differences in the  $S = 1$  channel from the previous discussion due to the mixing in the initial  ${}^3S_1$ - ${}^3S_1^*$  scattering state and final  ${}^3P_2$ - ${}^3P_2^*$  bound state. The scattering state contribution scales as  $\mathcal{A}^{(11)}(B_0 + J_0)$ ,  $\mathcal{A}^{(12)}(B_0 + J_0)$ . In the  $S = 1$  channel,  $a_0^{(1)} \sim 1/\Lambda$  and assuming all the scattering length parameters  $a_{11} \sim a_{12} \sim a_{22} \sim 1/\Lambda$  to be natural as well, we see from Eq. (14) that the initial state interaction in this channel also scales as  $Q/\Lambda$  compared to the contributions Fig. 1 (a), (c) without initial state interaction. Thus in this theory also the scaling for the  $s$ -wave interaction is similar to the theory without explicit  ${}^7\text{Li}^*$  degree of freedom up to NLO. There is one difference, however, from before. Now we have two wave function

renormalization constants  $\mathcal{Z}^{(^3P_2)}$ ,  $\mathcal{Z}^{(^3P_2^*)}$  that are shown in Eq. (20). Given that the ANCs for  $^3P_2$  and  $^3P_2^*$  [32, 50] are of similar size, we do not attempt any perturbative expansion in the mixing parameter  $r_{12}$ .

To summarize, the LO contribution to the capture to the  $2^+$  ground state is from the spin  $S = 2$  channel. At this order the cross section depends only on the  $^5S_2$  scattering length  $a_0^{(2)}$  and the  $^5P_2$  effective momentum  $r_1^{(^5P_2)}$  in both EFT and EFT $_{\star}$ . The NLO corrections come from the  $^5S_2$  effective range  $r_0^{(2)}$  and from the capture in the spin  $S = 1$  channel without initial interaction in either of the two theories, EFT or EFT $_{\star}$ . Thus the momentum dependence in EFT and EFT $_{\star}$  are indistinguishable at NLO. Up to this order, the difference between the two theories lies in the interpretation of the wave function renormalization constant  $\mathcal{Z}^{(^3P_2)}$ —in the EFT without  $^7\text{Li}^*$  one directly relates  $\mathcal{Z}^{(^3P_2)}$  with the  $p$ -wave effective momentum  $r_1^{(^3P_2)}$ . In EFT $_{\star}$ ,  $\mathcal{Z}^{(^3P_2)}$  (and  $\mathcal{Z}^{(^3P_2^*)}$ ) is a function of three effective momenta  $r_{11}$ ,  $r_{12}$ ,  $r_{22}$ .

The proposed power counting for the capture to the  $1^+$  state of  $^8\text{Li}$  in this work is very similar.

## VI. RESULTS AND ANALYSIS

In Fig. 4, the EFT/EFT $_{\star}$  Lynn LO curve was generated by constraining the wave function renormalization constant  $\mathcal{Z}^{(^5P_2)}$  from the thermal capture data [6]. We use the zed-parameterization. The fitted effective momentum  $r_1^{(^5P_2)}$  value is in Table I. We took  $a_0^{(2)} = -3.63(5)$  fm [46]. At NLO, the wave function renormalization  $\mathcal{Z}^{(^3P_2)}$  was constrained by the ratio of the ANCs  $C_{1,^3P_2}^2/C_{1,^5P_2}^2 = 0.228(42)$  fm $^{-1}$  [47], and then  $\mathcal{Z}^{(^5P_2)}$  was fitted to thermal capture data. This is the curve labeled EFT/EFT $_{\star}$  Lynn-ANC NLO in Fig. 4. As discussed earlier, see Fig. 2, it is important to independently constrain the wave function renormalization constants in the  $S = 2$  and  $S = 1$  channels since the capture data and the branching ratio are not sufficient. We see a large change in the  $r_1^{(^5P_2)}$  value at NLO as expected in the zed-parameterization, see Table I.  $\mathcal{Z}^{(^3P_2)}$  can be expressed in terms of a single effective momentum in EFT but in EFT $_{\star}$  it depends on three effective momenta. As mentioned earlier, we do not attempt to write  $\mathcal{Z}^{(^3P_2)}$  in terms of these effective momenta. The LO and NLO curves and the error bands, from errors in the input parameters only, overlap. This is primarily a consequence of constraining both the LO and NLO results to the same thermal capture data. As alternative fitting procedure one determines the unknown couplings from just the ANCs, like the last two rows of Table I. The errors in Fig. 4 were propagated in quadrature from the errors in the input parameters.

In the bottom panel of Fig. 4, we show only the error associated with varying the  $s$ -wave effective range  $r_0^{(2)} \sim 1/\Lambda$  in the  $^5S_2$  channel in the range  $-5$  fm to  $5$  fm.  $r_0^{(2)}$  has a noticeable impact on the capture cross section only at larger momenta where precision data is lacking, and also happens to be in a momentum range where the  $3^+$  resonance contribution is significant. The resonance contribution can be added in EFT as discussed earlier [31]. In this work we only include the non-resonant contribution.

The plot in Fig. 5 includes capture to both the  $2^+$  ground- and  $1^+$  excited-state of  $^8\text{Li}$  at NLO. The  $2^+$  capture cross section is the same as in Fig. 4. The wave function renormalization constant  $\mathcal{Z}^{(^3P_1)}$  in the  $1^+$  capture is constrained from the ratio  $C_{1,^3P_1}^2/C_{1,^5P_1}^2 = 0.73(12)$  fm $^{-1}$  [47], and  $\mathcal{Z}^{(^5P_1)}$  to the thermal capture data [6]. We include the expected 10%

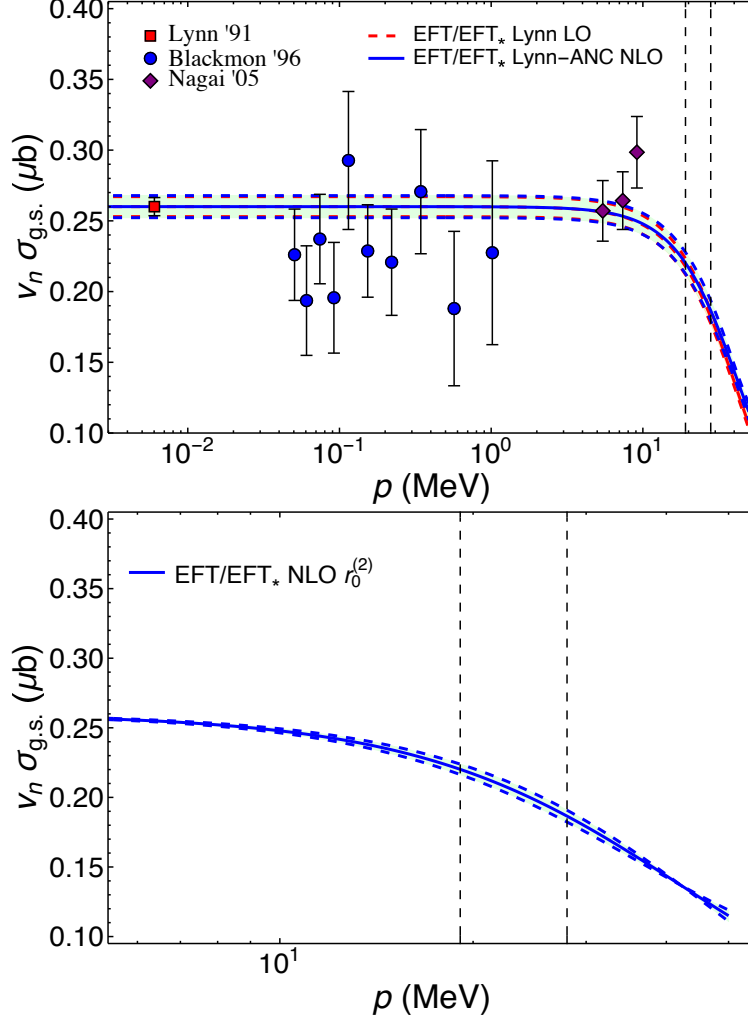


FIG. 4. Capture cross section to the  $2^+$  state. The LO (red) dashed and NLO (blue) solid curves, and error bands (red dashed and blue dashed curves) overlap. Both of these were constrained by thermal capture data [6]. We varied  $r_0^{(2)}$  in the range  $-5$  fm to  $5$  fm. The bottom panel shows only the variation due to  $r_0^{(2)}$ . The grid lines are at the  $3^+$  resonance momentum  $p_R = 19.1$  MeV and the  ${}^7\text{Li}^*$  inelasticity  $\gamma_\Delta = 28.0$  MeV.

EFT/EFT $_{\star}$  error in Fig. 5 from NNLO corrections. We show some parameters for the capture to  $1^+$  in Table II. As in the  $2^+$  capture, we express the wave function renormalization only in the spin  $S = 2$  channel  $\mathcal{Z}^{(5P_1)}$  in terms of an effective momentum  $r_1^{(5P_1)}$ . We see that the extrapolation of the EFT/EFT $_{\star}$  curves to low momentum gives an accurate postdiction of the sub-thermal datum [8].

The higher momentum data points in Fig. 5 from Refs. [8, 9] are associated with the M1 transition from the initial  $3^+$  resonance state. As mentioned before, this contribution can be included in EFT as presented in Ref. [31] where the resonance is described as a  ${}^5P_3$  state of the valance neutron and the ground state of  ${}^7\text{Li}$ . The excited state  ${}^7\text{Li}^*$  does not contribute to the initial  ${}^5P_3$  scattering state. To keep the discussion more focused we do not include the M1 contribution.



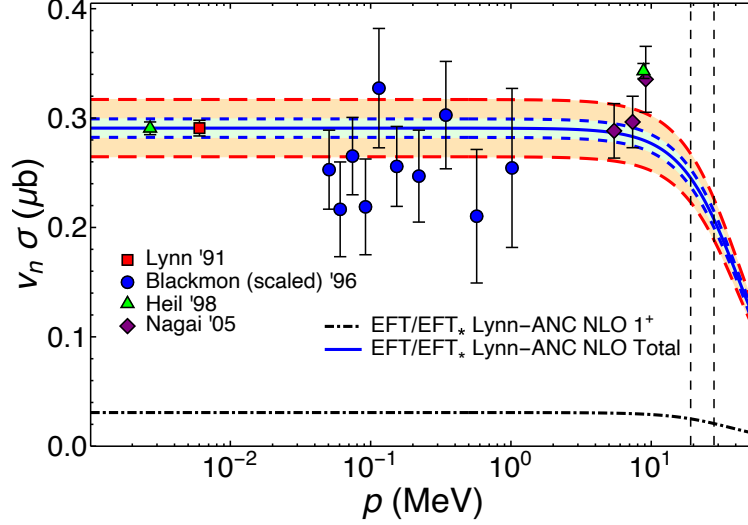


FIG. 5. Total capture cross section to the  $2^+$  and  $1^+$  state at NLO. Both of these were constrained by the thermal capture data [6]. We varied  $r_0^{(2)}$  in the range  $-5$  fm to  $5$  fm. The (blue) shaded region between the (blue) dashed curves shows the error due to the input parameters. The (reddish) band between the (red) long-dashed curves indicate the 10% NNLO EFT errors. The (blue) solid curve is the total NLO result and the (black) dot-dashed curve is the NLO capture to the  $1^+$  state. The error bands in the capture to the  $1^+$  state are not shown but included in the total capture cross section. The grid lines are at the  $3^+$  resonance momentum  $p_R = 19.1$  MeV and the  ${}^7\text{Li}^*$  inelasticity  $\gamma_\Delta = 28.0$  MeV. Ref. [7] measured capture to the  $2^+$  ground state which was scaled in that work by a factor of  $1/0.894$  to represent the total capture rate.

TABLE II.  ${}^7\text{Li}(n, \gamma){}^8\text{Li}$  capture to the  $1^+$  state. We estimate the parameters as described in the text. Thermal ratio is the EFT cross section normalized to Lynn data [6]. Branching ratio is capture in the  $S = 2$  spin channel compared to the total cross section at thermal momentum. We corrected the  $p$ -wave effective momenta values from Ref. [31] in EFT A below. We show results to 3 significant figures.

Theory	$r_1^{(5P_1)}$ (fm $^{-1}$ )	$\mathcal{Z}_1^{(5P_1)}$	$\mathcal{Z}_1^{(3P_1)}$	Thermal ratio	Branching ratio
EFT A	$-2.36(36)$	$1.93(32)$	$1.93(32)$	1	$0.937(18)$
EFT/EFT $_{\star}$ Lynn LO	$-1.62(17)$	$2.56(27)$	—	1	1
EFT/EFT $_{\star}$ Lynn-ANC NLO	$-2.36(19)$	$2.41(27)$	$1.77(29)$	1	$0.912(20)$
EFT/EFT $_{\star}$ ANC LO	$-1.88(16)$	$2.22(19)$	—	$0.865(74)$	1
EFT/EFT $_{\star}$ ANC NLO	$-2.51(16)$	$2.22(19)$	$1.63(22)$	$0.921(75)$	$0.914(17)$

Finally in Fig. 6, we consider some recent Coulomb dissociation data that was used to predict the capture cross section. We extracted the experimental results digitally from Fig. 10 of Ref. [51]. We assumed the lowest horizontal-axis tick mark on the log-log plot to be at 10 keV (instead of 1 keV) which gives the expected results for the known Nagai [9] data. We expect our digital extraction to introduce errors of about a 1%. The dashed (red) curve is the EFT A result from Fig. 3 with the capture from initial  $d$ -wave states included that was published earlier [30, 31]. This is not a complete NNLO calculation in the EFT

without  ${}^7\text{Li}^*$  core as it lacks a two-body contribution and  $S = 2$  channel  $s$ -wave effective range correction. However, one can see that the expected NNLO corrections to the NLO EFT/EFT $_{\star}$  solid (blue) curve from Fig. 5 moves the theory result in better agreement with the data. The differences between the dashed and solid curve are about 4% at  $E \approx 1$  MeV which is consistent with a NNLO correction.

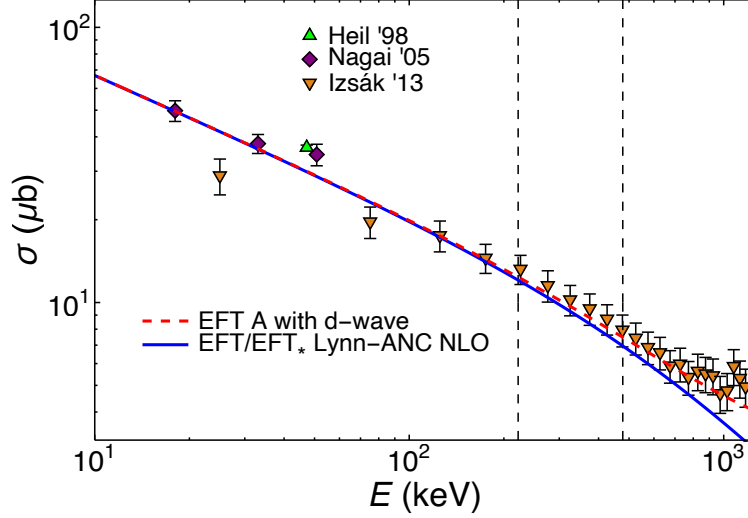


FIG. 6. Capture cross section via Coulomb dissociation. The Izsák data was extracted from Ref. [51] as explained in the text. The dashed (red) curve is the EFT A result from Fig. 3 together with capture from  $d$ -wave initial state [30, 31]. Solid (blue) curve is the NLO EFT/EFT $_{\star}$  result from Fig. 5.

## VII. CONCLUSIONS

We considered the E1 contribution to the  ${}^7\text{Li}(n, \gamma){}^8\text{Li}$  capture reaction at low energies. A coupled-channel calculation for the contribution from the excited  ${}^7\text{Li}^*$  core was presented. This theory was compared to an earlier calculation which did not include the excited core as an explicit degree of freedom [30, 31]. We developed a power counting for both the EFTs—one with explicit excited  ${}^7\text{Li}^*$  core and one without—and show that the two theories are equivalent in their momentum-dependence up to NLO. This confirms the expectation that the  ${}^7\text{Li}^*$  contribution which participates only in the sub-dominant spin  $S = 1$  channel with a branching ratio of  $\sim 0.2$  is a higher-order effect [30, 31]. Though the momentum dependence in both EFTs at this order is the same, the interpretation of the cross section in the  $S = 1$  channel in terms of  $p$ -wave effective momenta in the two theories is different. In the EFT without  ${}^7\text{Li}^*$ , we can relate the cross section to an overall normalization in terms of the  ${}^3P_2$  effective momentum. No such simple interpretation is possible in the other EFT $_{\star}$  with the excited  ${}^7\text{Li}^*$  core. We estimate the theoretical errors in our calculation to be about 10% from  $Q^2/\Lambda^2$  NNLO corrections.

The survey presented in Sec. IV relaxed the simplification  $r_1^{(3P_2)} = r_1^{(5P_2)} \sim \Lambda$ , for the  $2^+$   ${}^8\text{Li}$  ground state, done in previous works [30, 31]. In the EFT without  ${}^7\text{Li}^*$ , Fig. 2 shows how  $r_1^{(3P_2)}$  and  $r_1^{(5P_2)}$  are correlated to reproduce a given value for the thermal capture to the

ground  $2^+$  state of  $^8\text{Li}$  and the branching ratio of the spin channel  $S = 2$ . The differences from the simplified assumption is compatible with a higher-order correction. Alternatively  $r_1^{(^3P_2)}$  and  $r_1^{(^5P_2)}$  can be fixed via the corresponding ANCs  $C_{1,^3P_2}^2$  and  $C_{1,^5P_2}^2$  calculated in Ref. [50] or taken from experiment [47], with similar numerical results. In the  $\text{EFT}_\star$  with explicit  $^7\text{Li}^\star$  the wave function renormalization constants  $\mathcal{Z}^{(^5P_2)}$ ,  $\mathcal{Z}^{(^3P_2)}$ , and  $\mathcal{Z}^{(^3P_2^\star)}$  can be fitted to the corresponding ANCs, though they are not enough to pin down the extra EFT couplings that appear with the excited core as an explicit degree of freedom—while  $r_1^{(^5P_2)}$  is uniquely determined from  $\mathcal{Z}^{(^5P_2)}$ , this is not true for the three  $S = 1$  effective momenta  $r_{ij}$  in terms of  $\mathcal{Z}^{(^3P_2)}$  and  $\mathcal{Z}^{(^3P_2^\star)}$ . Similar analysis for the  $p$ -wave channels corresponding to the  $1^+$   $^8\text{Li}$  excited state holds.

At NNLO, there are several contributions to the capture to the  $2^+$  ground state of  $^8\text{Li}$ . Two-body current contribution to capture from  $s$ -wave scales as  $k_0 a_0^{(2)} L_{\text{E1}}$  [52]. This is a  $Q^2/\Lambda^2$  NNLO contribution for a natural-sized coupling  $L_{\text{E1}} \sim 1$ , given the scalings for the scattering length  $a_0^{(2)} \sim 1/Q$  and the photon energy  $k_0 = (p^2 + \gamma_0^2)/(2\mu) \sim Q^3/\Lambda^2$ . The contributions from the  $S = 1$  channel start with initial state  $s$ -wave strong interactions. In the EFT without  $^7\text{Li}^\star$  core, the  $s$ -wave interactions can be parameterized by the scattering length  $a_0^{(1)}$ . In the  $\text{EFT}_\star$  with  $^7\text{Li}^\star$  core, the initial state  $s$ -wave interactions involve a coupled-channel calculation parameterized by the three scattering lengths  $a_{11}$ ,  $a_{12}$ ,  $a_{22}$ . Capture from  $d$ -wave that scales as  $p^4/(p^2 + \gamma_0)^2$  was included in Refs. [30, 31]. However, it is kinematically suppressed at low momentum, contributing around 10% at  $p \gtrsim 40$  MeV. So this contribution can also be included as NNLO in the dominant spin  $S = 2$  channel. In the same spin channel the initial state  $^5S_2$  receives a NNLO correction from two insertions of the leading derivative coupling proportional to  $[a_0^{(2)} r_0^{(2)} p^2/2]^2$  while the shape parameter  $\mathcal{P}_0^{(2)}$  enters at N<sup>3</sup>LO. The NNLO contributions for the capture to the  $1^+$  excited state of  $^8\text{Li}$  are similar.

The EFT formalism and the theory expressions for the cross section in this work, with the excited  $^7\text{Li}^\star$  core contributions, are different from those in Ref. [32]. We also differ in the interpretation of the wave function renormalization constants in terms of the  $p$ -wave scattering parameters. However, given that the excited  $^7\text{Li}^\star$  core contributions to the momentum dependence of the cross section are a NNLO effect, it is expected that the numerical results of Ref. [32] are similar to those obtained here which in turn do not differ significantly (differences  $\lesssim 1.5\%$  for  $p \lesssim 40$  MeV) from earlier calculations (excluding  $d$ -wave contributions) in Refs. [30, 31].

In this work, we only included the non-resonant capture. Future work would include the M1 contribution from the  $3^+$  resonance to  $^7\text{Li}(n, \gamma)^8\text{Li}$  reaction [36]. We would also apply our formalism to the related capture reaction  $^7\text{Be}(p, \gamma)^8\text{B}$ .

## ACKNOWLEDGMENTS

We thank C. Bertulani and A. Horváth for discussing their work on Coulomb dissociation with us. This work was supported in part by U.S. NSF grants PHY-1615092 and PHY-1913620 (PP, GR) and Brazilian agency FAPESP thematic projects 2017/05660-0 and 2019/07767-1, and INCT-FNA Proc. No. 464898/2014-5 (RH). The cross section figures for this article have been created using SciDraw [53].

## Appendix A: Projectors

The following are from Ref. [31] that we include for reference. For each partial wave we construct the corresponding projection operators from the relative core-nucleon velocity, the spin-1/2 Pauli matrices  $\sigma_i$ 's, and the following spin-1/2 to spin-3/2 transition matrices

$$\begin{aligned} S_1 &= \frac{1}{\sqrt{6}} \begin{pmatrix} -\sqrt{3} & 0 & 1 & 0 \\ 0 & -1 & 0 & \sqrt{3} \end{pmatrix}, \\ S_2 &= -\frac{i}{\sqrt{6}} \begin{pmatrix} \sqrt{3} & 0 & 1 & 0 \\ 0 & 1 & 0 & \sqrt{3} \end{pmatrix}, \\ S_3 &= \frac{2}{\sqrt{6}} \begin{pmatrix} 0 & 1 & 0 & 0 \\ 0 & 0 & 1 & 0 \end{pmatrix}, \end{aligned} \quad (\text{A1})$$

which satisfy

$$S_i S_j^\dagger = \frac{2}{3} \delta_{ij} - \frac{i}{3} \epsilon_{ijk} \sigma_k, \quad S_i^\dagger S_j = \frac{3}{4} \delta_{ij} - \frac{1}{6} \{J_i^{(3/2)}, J_j^{(3/2)}\} + \frac{i}{3} \epsilon_{ijk} J_k^{(3/2)}, \quad (\text{A2})$$

where  $J_i^{(3/2)}$ 's are the generators of the spin-3/2. We construct the Clebsch-Gordan coefficient matrices

$$F_i = -\frac{i\sqrt{3}}{2} \sigma_2 S_i, \quad Q_{ij} = -\frac{i}{\sqrt{8}} \sigma_2 (\sigma_i S_j + \sigma_j S_i), \quad (\text{A3})$$

for projections onto spin channels  $S = 1$  and  $S = 2$ , respectively. Then in coordinate space the relevant projectors that appear in the Lagrangians involving the  ${}^7\text{Li}$  ground state in Eqs. (1), (2) are [30, 31]

$$\begin{aligned} P_i^{(3S_1)} &= F_j, & P_{ij}^{(5S_2)} &= Q_{ij}, \\ P_i^{(3P_1)} &= \sqrt{\frac{3}{2}} F_x \left( \frac{\vec{\nabla}}{m_c} - \frac{\overleftarrow{\nabla}}{m_n} \right)_y \epsilon_{ixy}, & P_{ij}^{(3P_2)} &= \sqrt{3} F_x \left( \frac{\vec{\nabla}}{m_c} - \frac{\overleftarrow{\nabla}}{m_n} \right)_y R_{xyij}, \\ P_i^{(5P_1)} &= \sqrt{\frac{9}{5}} Q_{ix} \left( \frac{\vec{\nabla}}{m_c} - \frac{\overleftarrow{\nabla}}{m_n} \right)_x, & P_{ij}^{(5P_2)} &= \frac{1}{\sqrt{2}} Q_{xy} \left( \frac{\vec{\nabla}}{m_c} - \frac{\overleftarrow{\nabla}}{m_n} \right)_z T_{xyzij}. \end{aligned} \quad (\text{A4})$$

The tensors

$$\begin{aligned} R_{ijxy} &= \frac{1}{2} \left( \delta_{ix} \delta_{jy} + \delta_{iy} \delta_{jx} - \frac{2}{3} \delta_{ij} \delta_{xy} \right), \\ T_{xyzij} &= \frac{1}{2} \left( \epsilon_{xzi} \delta_{yj} + \epsilon_{xzy} \delta_{ji} + \epsilon_{yzi} \delta_{xj} + \epsilon_{yzj} \delta_{xi} \right), \end{aligned} \quad (\text{A5})$$

ensures total angular momentum  $j = 2$  is picked.

The new projectors to describe the interactions in Eq. (2) with the excited  ${}^7\text{Li}^*$  core are

$$\begin{aligned} P_i^{(3S_1^*)} &= \frac{1}{\sqrt{2}} \sigma_i, \\ P_i^{(3P_1^*)} &= \frac{\sqrt{3}}{2} \sigma_x \left( \frac{\vec{\nabla}}{m_c} - \frac{\overleftarrow{\nabla}}{m_n} \right)_y \epsilon_{ixy}, & P_{ij}^{(3P_2^*)} &= \sqrt{\frac{3}{2}} \sigma_x \left( \frac{\vec{\nabla}}{m_c} - \frac{\overleftarrow{\nabla}}{m_n} \right)_y R_{xyij}. \end{aligned} \quad (\text{A6})$$

For the external states we introduce the photon vector ( $\varepsilon_i^{(\gamma)}$ ), excited state  ${}^8\text{Li } 1^+$  spin-1 ( $\varepsilon_j$ ), and ground state  ${}^8\text{Li } 2^+$  spin-2 ( $\varepsilon_{ij}$ ) polarizations, obeying the following polarization sums [54, 55],

$$\sum_{\text{pol.}} \varepsilon_i^{(\gamma)} \varepsilon_j^{(\gamma)*} = \delta_{ij} - \frac{k_i k_j}{k^2}, \quad \sum_{\text{pol. ave.}} \varepsilon_i \varepsilon_j^* = \frac{\delta_{ij}}{3}, \quad \sum_{\text{pol. ave.}} \varepsilon_{ij} \varepsilon_{lm}^* = \frac{R_{ijlm}}{5}. \quad (\text{A7})$$

- 
- [1] M. Wiescher, F. Käppeler, and K. Langanke, *Annu. Rev. Astron. Astrophys.* **50**, 165 (2012).
  - [2] C. R. Brune and B. Davids, *Ann. Rev. Nucl. Part. Sci.* **65**, 87 (2015).
  - [3] C. Bertulani and A. Gade, *Phys. Rept.* **485**, 195 (2010), arXiv:0909.5693 [nucl-th].
  - [4] L. H. Kawano, W. A. Fowler, R. W. Kavanagh, and R. A. Malaney, *Astrophys. J.* **372**, 1 (1991).
  - [5] D. J. Hughes, D. Hall, C. Egger, and E. Goldfarb, *Phys. Rev.* **72**, 646 (1947).
  - [6] J. E. Lynn, E. T. Jurney, and S. Raman, *Phys. Rev. C* **44**, 764 (1991).
  - [7] J. C. Blackmon *et al.*, *Phys. Rev. C* **54**, 383 (1996).
  - [8] M. Heil, F. Käppler, M. Wiescher, and A. Mengoni, *Astrophys. J.* **507**, 1002 (1998).
  - [9] Y. Nagai *et al.*, *Phys. Rev. C* **71**, 055803 (2005).
  - [10] R. Izsák *et al.*, *Phys. Rev. C* **88**, 065808 (2013), arXiv:1312.3498 [nucl-ex].
  - [11] P. Navratil, R. Roth, and S. Quaglioni, *Phys. Rev. C* **82**, 034609 (2010), arXiv:1007.0525 [nucl-th].
  - [12] K. Bennaceur, F. Nowacki, J. Okolowicz, and M. Ploszajczak, *Nucl. Phys. A* **651**, 289 (1999), arXiv:nucl-th/9901060.
  - [13] K. Fosse, N. Michel, M. Płoszajczak, Y. Jaganathen, and R. Id Betan, *Phys. Rev. C* **91**, 034609 (2015), arXiv:1502.01631 [nucl-th].
  - [14] P. Descouvemont and D. Baye, *Nucl. Phys. A* **567**, 341 (1994).
  - [15] T. Tombrello, *Nucl. Phys.* **71**, 459 (1965).
  - [16] A. Aurdal, *Nuclear Physics A* **146**, 385 (1970).
  - [17] H. Esbensen, *Phys. Rev. C* **70**, 047603 (2004).
  - [18] F. C. Barker, *Nucl. Phys.* **A768**, 241 (2006).
  - [19] B. Davids and S. Typel, *Phys. Rev. C* **68**, 045802 (2003), arXiv:nucl-th/0304054.
  - [20] S. Typel and G. Baur, *Nucl. Phys.* **A759**, 247 (2005), arXiv:nucl-th/0411069.
  - [21] C. Bertulani, *Z. Phys. A* **356**, 293 (1996).
  - [22] J. T. Huang, C. A. Bertulani, and V. Guimaraes, *At. Data Nuc. Data Tables* **96**, 824 (2010), arXiv:0810.3867 [nucl-th].
  - [23] N. Shul'gina, B. Danilin, V. Efros, J. Bang, J. Vaagen, and M. Zhukov, *Nucl. Phys. A* **597**, 197 (1996).
  - [24] L. Grigorenko, B. Danilin, V. Efros, N. Shul'gina, and M. Zhukov, *Phys. Rev. C* **60**, 044312 (1999).
  - [25] C. Bertulani, H. Hammer, and U. van Kolck, *Nucl. Phys. A* **712**, 37 (2002), arXiv:nucl-th/0205063.
  - [26] P. Bedaque, H. Hammer, and U. van Kolck, *Phys. Lett. B* **569**, 159 (2003), arXiv:nucl-th/0304007.
  - [27] G. Rupak, *Int. J. Mod. Phys. E* **25**, 1641004 (2016).

- [28] H. W. Hammer, C. Ji, and D. Phillips, J. Phys. G **44**, 103002 (2017), arXiv:1702.08605 [nucl-th].
- [29] H.-W. Hammer, S. König, and U. van Kolck, Rev. Mod. Phys. **92**, 025004 (2020), arXiv:1906.12122 [nucl-th].
- [30] G. Rupak and R. Higa, Phys. Rev. Lett. **106**, 222501 (2011), arXiv:1101.0207 [nucl-th].
- [31] L. Fernando, R. Higa, and G. Rupak, Eur. Phys. J. A **48**, 24 (2012), arXiv:1109.1876 [nucl-th].
- [32] X. Zhang, K. M. Nollett, and D. Phillips, Phys. Rev. C **89**, 024613 (2014), arXiv:1311.6822 [nucl-th].
- [33] T. D. Cohen, B. A. Gelman, and U. van Kolck, Phys. Lett. B **588**, 57 (2004), arXiv:nucl-th/0402054.
- [34] V. Lensky and M. Birse, Eur. Phys. J. A **47**, 142 (2011), arXiv:1109.2797 [nucl-th].
- [35] D. Tilley, J. Kelley, J. Godwin, D. Millener, J. Purcell, C. Sheu, and H. Weller, Nuclear Physics A **745**, 155 (2004).
- [36] R. Higa, P. Premarathna, and G. Rupak, Under publication.
- [37] W. J. Huang, G. Audi, M. Wang, F. G. Kondev, S. Naimi, and X. Xu, Chinese Physics **C41**, 030002 (2017).
- [38] M. Wang, G. Audi, F. G. Kondev, W. J. Huang, S. Naimi, and X. Xu, Chinese Physics **C41**, 030003 (2017).
- [39] H. W. Griesshammer, Nucl. Phys. A **744**, 192 (2004), arXiv:nucl-th/0404073.
- [40] D. Tilley, C. Cheves, J. Godwin, G. Hale, H. Hofmann, J. Kelley, C. Sheu, and H. Weller, Nuclear Physics A **708**, 3 (2002).
- [41] Y. G. Abov, O. N. Yermakov, A. D. Gul'ko, P. A. Krupchitsky, and S. S. Trostin, Nucl. Phys. **34**, 505 (1962).
- [42] D. Connor, Phys. Rev. Lett. **3**, 429 (1959).
- [43] A. Gul'ko, S. Trostin, and A. Hudoklin, Sov. J Nucl. Phys. **6**, 477 (1968).
- [44] D. B. Kaplan, M. J. Savage, and M. B. Wise, Phys. Lett. B **424**, 390 (1998), arXiv:nucl-th/9801034.
- [45] H. Knox and R. Lane, Nucl. Phys. A **359**, 131 (1981).
- [46] L. Koester, K. Knopf, and W. Waschkowski, Z. Phys. **A312**, 81 (1983).
- [47] L. Trache, A. Azhari, F. Carstoiu, H. Clark, C. Gagliardi, Y. Lui, A. Mukhamedzhanov, X. Tang, N. Timofeyuk, and R. Tribble, Phys. Rev. C **67**, 062801 (2003), arXiv:nucl-ex/0304016.
- [48] F. Barker, Nucl. Phys. A **588**, 693 (1995).
- [49] D. R. Phillips, G. Rupak, and M. J. Savage, Phys. Lett. B **473**, 209 (2000), arXiv:nucl-th/9908054.
- [50] K. M. Nollett and R. Wiringa, Phys. Rev. C **83**, 041001 (2011), arXiv:1102.1787 [nucl-th].
- [51] R. Izsak *et al.*, Phys. Rev. C **88**, 065808 (2013), arXiv:1312.3498 [nucl-ex].
- [52] R. Higa, G. Rupak, and A. Vaghani, Eur. Phys. J. A **54**, 89 (2018), arXiv:1612.08959 [nucl-th].
- [53] M. A. Caprio, Comput. Phys. Commun. **171**, 107 (2005), <http://scidraw.nd.edu>.
- [54] S. Choi, J. Lee, J. S. Shim, and H. Song, J. Korean Phys. Soc. **25**, 576 (1992).
- [55] S. Fleming, T. Mehen, and I. W. Stewart, Nucl. Phys. **A677**, 313 (2000), arXiv:nucl-th/9911001.